Doppler robustness of joint communication and radar systems using the Wiener filter

Jean-Yves Baudais, Stéphane Méric, Bochra Benmeziane, Kevin Cinglant

Doppler robustness of joint communication and radar systems using the Wiener filter

Jean-Yves Baudais, Stéphane Méric, Bochra Benmeziane and Kevin Cinglant

***Abstract*—The orthogonal frequency-division multiplexing (OFDM) is a promising waveform for joint radar and communication systems. In this article, a unified approach is proposed to analyse both radar and communication robustness with respect to Doppler mismatch. The analytical study leads to an expression that links the radar performance to the communication one. The performance of a delay-Doppler radar is quantified by modelling the delay response of the OFDM radar with an appropriate random variable. Different delay filters are analysed, among which the Wiener filter. The analytical results are validated by simulations, they show that the radar system benefits from the Wiener filter, and the configurations where this filter outperforms the other ones are outlined.**

***Index Terms*—Joint radar communication, OFDM, delay-Doppler radar, Wiener filter, SINR, PSLR.**

I. Introduction

The orthogonal frequency-division multiplexing (OFDM) is one of the waveforms used to allow joint radar and communication (JRC) applications, especially in automotive contexts [1]–[4]. To ensure both radar and communication capabilities, two dual-function radar communication (DFRC) strategies are commonly proposed: a modulated radar signal to transmit information bits, or a radar signal processing based on wireless communication waveforms. Both strategies lead to many designs, optimisations and solutions, depending on many parameters [3], [5]. This article investigates the latter strategy based on the OFDM signal.

Both communication and radar systems suffer various causes of degradation, among which the Doppler is the one we are interested in. In communication systems, the Doppler shift degrades the signal-to-interference plus noise ratio (SINR), a key parameter that characterises the quality of the transmission. The receiver estimates and compensates the common frequency offset (CFO) due to this Doppler, reducing the residual CFO, or the corresponding residual Doppler shift, as low as possible [6]. In radar systems, the Doppler shift can be an estimated parameter. This is the case with delay-Doppler radar, considered in this article. The performance of this radar is based on the OFDM signal parameters [7], and on its ambiguity function [8]. However, large Doppler values lead to a mismatch loss that degrades the property of the ambiguity function, or of the delay-Doppler response, and reduces the detection capabilities [9]. The radar performance impacted by the Doppler shift has already been evaluated in the case of the studied OFDM signal [10], [11]. All these results are based on simulations and no link is drawn between the two parts of the JRC system, according to our knowledge. We then propose a unified analytical study that evaluates the Doppler mismatch loss in both radar and communication systems in JRC context.

The JRC performance is not only affected by the Doppler mismatch, but also affected by the filter used at the receiver side. The conventional radar filter is the matched filter (MF) that minimises the signal-to-noise ratio (SNR) of the main lobe of the delay-Doppler response. The zero-forcing filter (ZF) is also introduced as a mismatched filter to recover the orthogonality or to improve the side-lobe structure [9]. In the JRC context, it is also used to recover the channel impulse response, regardless of the transmitted data [1]. We propose to apply another filter: the Wiener filter (WF), also called the linear minimum mean square error filter, widely used in communication systems. This filter is also used in radar systems to improve the delay resolution [12], or to reduce the interference [13]. However, the robustness of this filter has never been analysed in the JRC context, up to our knowledge. We show in this article how the Doppler shift affects the performance of the WF, and how it outperforms the two other filters, combining the advantages of these two filters. By modelling the OFDM delay-Doppler response as a random variable (r.v.), the analytical study leads to a simple performance formula, validated by simulations in a wide range of configurations. The Doppler mismatch loss is quantified and we show how it depends on the filter used, and on the OFDM signal parameters. The study conducted for both radar and communication systems exhibits the dependence of the performance between both systems.

Contributions: The key contributions of this paper are the analysis of the Doppler mismatch and the use of the WF in JRC context:

- The OFDM JRC system is considered with the Doppler shift of a moving environment or a moving JRC system. To the best of our knowledge, the unified analytical derivation of the Doppler mismatch proposed in this article has never been conducted for both radar and communication systems;
- The WF is considered as a potential replacement of the MF or ZF for range estimation, or short time processing. This filter has widely been studied for spread-spectrum OFDM communication systems as channel equaliser with one coefficient per subcarrier.

J.-Y. Baudais and S. Méric are with Univ Rennes, INSA Rennes, CNRS, IETR-UMR 6164, F-35000 Rennes, France (email: jean-yves.baudais@insa-rennes.fr).

B. Benmeziane and K. Cinglant are with ZF Autocruise, 29280 Plouzané, France

The analytical expression of its performance is derived in this article;
- The obtained analytical expressions characterise both radar and communication systems, they are simple and accurate to be used to design the JRC systems.

The rest of this article is organised as follows. Section II introduces both communication and radar OFDM systems. The three filters studied are presented in Section III. The main results are developed in Section IV where the Doppler effect on the delay response is modelled. These results are applied in Section V to the peak-side-lobe ratio (PSLR) and integrated-side-lobe ratio (ISLR) of radar systems, to SINR metric used in communication systems, and in Section VI to sparse OFDM signals. Section VII gives some examples to illustrate and quantify the analytical study. The consequences on JRC system design are drawn in Section VIII. The conclusion closes the article, in Section IX.

II. Joint radar and communication system

We consider a JRC system with the DFRC, where only one waveform is used. Both radar and communication systems are combined on a unique platform, with the same radio frequency and base-band hardware [2]. The signal, transmitted for communication purpose, is reflected back to the transmitter by the target and processed for radar applications. Before developing the signal expressions, we give some inputs on the considered JRC context.

A. Scenario

The typical scenario is done with two JRC platforms. Both can

- transmit OFDM signals,
- receive and process OFDM signals for the communication purpose,
- receive and process OFDM signals for the radar application.

The signal transmitted by the first JRC platform is received by the second one, for communication applications between the two platforms. This signal is also reflected back by the environment to the first JRC platform and processed for radar applications. The tasks of the two platforms can be exchanged and the first platform can received the signal transmitted by the second one. With multiple JRC platforms in a given electromagnetic area, centralised or mobile ad-hoc networks can be used to share the space-time-frequency resource among the platforms, and to synchronise the network [14]. To simplify the analysis in our study, we consider a space-time-frequency elementary resource used by only one JRC platform at a time to transmit the signal. This ensures an orthogonal transmission-reception and an interference free signal processing. The radar system is a mono-static one and, unlike [15], the same system is used for uplink and downlink radar applications.

B. Communication system

The OFDM communication system is first considered. The signal is transmitted by one JRC platform and received by the other one. Let n be the number of sub-carriers, which transmit n complex symbols $a_{k,i} \in \mathbb{C}\backslash\{0\}$ during the time $t \in [0, T)$, where T is the time period of the OFDM symbols. The OFDM base-band symbol $k = 0$ with a rectangular pulse shaping is [6, § 1.2.1]

$$\tilde{x}_0(t) = \frac{1}{\sqrt{n}} \sum_{i=0}^{n-1} a_{0,i} e^{2\imath\pi f_i t}, \tag{1}$$

where f_i are the sub-carriers. The orthogonality is ensured with $f_i = \frac{i}{T}$. The bandwidth at -3 dB used to transmit the OFDM signal is $\frac{n}{T}$. A guard time, that is a cyclic prefix, of duration τ_g is added to maintain the periodicity for the signal processing at the receiver side, and to absorb the channel multi-path, or to combine multiple transmitted signals from different positions, as in the single frequency network of digital video broadcasting-terrestrial. The symbol $k = 0$ then writes

$$x_0(t) = \tilde{x}_0(t - \tau_g) = \frac{1}{\sqrt{n}} \sum_{i=0}^{n-1} a_{0,i} e^{2\imath\pi f_i (t-\tau_g)} \tag{2}$$

for $t \in [0, T + \tau_g)$, and zero otherwise. The OFDM transmission consists of multiple symbols and it is, with $t \in \mathbb{R}$ and $k \in \mathbb{Z}$,

$$x(t) = \sum_k x_k(t - k(T + \tau_g)) \,. \tag{3}$$

The analytical radio-frequency signal transmitted over the carrier f_c is

$$s(t) = x(t) e^{2\imath\pi f_c t} \,. \tag{4}$$

The following usual assumption is made.

Assumption 1. *The signal $x(t)$ is a narrow-band signal, i.e., $\max_i f_i \ll f_c$, with $i \in [0, n-1)$.*

Let the received base-band signal $y(t)$ be sampled without any synchronisation error nor delay, and normalised to be unit power. In this first derivation, the communication channel is considered Gaussian. The received signal is not processed by the JRC platform that has transmitted the signal, but by another one, the one to which the signal is intended. The useful part of the k-th OFDM symbol is given by $t \in [k(T + \tau_g) + \tau_g, (k + 1)(T + \tau_g))$, where the nominal OFDM sampling frequency is $\frac{n}{T}$. At $t = \frac{jT}{n} + k(T + \tau_g) + \tau_g$, the digital signal is

$$y_k(j) = \frac{1}{\sqrt{n}} \sum_{i=0}^{n-1} a_{k,i} e^{2\imath\pi \frac{ij}{n}} + b_k(j) \,, \tag{5}$$

with $b_k(j)$ the sample of the proper complex additive white Gaussian noise (AWGN). The signal is firstly OFDM demodulated with the Fourier transform, and the l-th corresponding sample of the k-th OFDM symbol is

$$Y_k(l) = \frac{1}{\sqrt{n}} \sum_{j=0}^{n-1} y_k(j) e^{-2\imath\pi \frac{jl}{n}} = a_{k,l} + B_k(l) \,, \tag{6}$$

where $B_k(l)$ is also AWGN with the same characteristics as $b_k(j)$.

Assumption 2. *The noise is a proper AWGN with zero mean and power* σ_b^2.

With synchronisation errors, due to oscillator mismatching or time varying channel, the Doppler shift appears. This frequency offset leads to inter-carrier interference that degrades the SNR, i.e., $Y_k(l)$ contains not only the $a_{k,l}$ symbol but also the other symbols $a_{k,l'}$, $l' \neq l$, transmitted by the other sub-carriers. The resulting SINR is [16], [17]

$$\gamma_{\text{SINR}} \approx \frac{1 - \frac{(\pi\tilde{\nu}T)^2}{3}}{\frac{1}{\gamma_{\text{SNR}}} + \frac{(\pi\tilde{\nu}T)^2}{3}} \tag{7}$$

with $\tilde{\nu}$ the residual Doppler shift after the frequency synchronisation, $\tilde{\nu}T$ the relative residual Doppler normalised by the sub-carrier spacing, and γ_{SNR} the input SNR. The SINR approximation (7) needs $\tilde{\nu}T < \frac{\sqrt{3}}{\pi}$, but in practice it is accurate only for $\tilde{\nu}T \leq \frac{1}{3}$. We provide in this article a new exact SINR expression for all Doppler values.

To ensure a low SNR degradation, the accuracy of the OFDM synchronisation should be better than 2 % of the carrier spacing [6, § 4.2.2.3]. Let us consider the IEEE 802.11p standard [18] as an example. The number of sub-carriers is $n = 64$ and, considering a 10 MHz signal bandwidth, the residual Doppler shift after frequency synchronisation should be less than 3 kHz. When the signal is also used for radar applications, the question that arises is what is the acceptable Doppler shift the radar system can support with low performance degradation. This question has already been tackled in the literature [11], [19], but we provide the first analytical derivation and a simple expression to calculate this degradation. Before answering this question, the radar system is presented.

C. Radar system

A mono-static delay-Doppler radar system is considered. The signal is transmitted by one JRC platform and received by the same one. The resolutions and ambiguities, which quantify the radar capabilities, are deduced from the characteristics of the OFDM signal [7]. However, these resolutions and ambiguities are not the purpose of this article. We focus on the OFDM signal transmitted, received and processed by the same JRC platform for radar applications. The OFDM signal, transmitted for communication applications in Section II-B, is reflected back to the radar by the target and received with the delay

$$\tau(t) = \frac{2d(t)}{c} = \tau_0 + \frac{2v}{c}(t - \tau_g)\,, \tag{8}$$

where $d(t)$ is the radar-target distance at time t, τ_0 is the delay at the phase origin[1], v is the radial speed of the target in a coordinate system attached to the radar, and c is the speed of light.

[1]For convenience sake, the origin of the phase is stated at $t = \tau_g$, as in (2).

The base-band received signal is, with (4),

$$\begin{aligned} y(t) &= Ae^{\imath\varphi_0} s(t - \tau(t)) e^{-2\imath\pi f_c t} + b(t) \\ &= Ae^{\imath\varphi_0} x(t - \tau(t)) e^{-2\imath\pi f_c \tau(t)} + b(t)\,. \end{aligned} \tag{9}$$

The path-loss and the target radar cross section (RCS) are characterised through $Ae^{\imath\varphi_0}$, with magnitude A and argument φ_0. As the target characteristics are not the point in this article, the analysis is simplified by considering a unit path-loss, unit and omnidirectional RCS, then $Ae^{\imath\varphi_0} = 1$. The usual radar signal processing considers $\tau(t)$ constant during one received symbol. It equals τ_k such as

$$\tau_k = \tau_0 + k(T + \tau_g)\frac{2v}{c} \tag{10}$$

for the k-th symbol. However, to evaluate the Doppler effect on the delay-Doppler response, we do not consider this usual assumption and take into account the waveform distortion introduced by the Doppler.

Using the IEEE 802.11p example and the practical rule of 2 % of the sub-carrier spacing introduced above, the target speed should check

$$v \leq \frac{0.02c}{2f_c T} = 79.5 \text{ m/s} \tag{11}$$

at 5.9 GHz to not increase the inter-carrier interference. However, this upper bound of the speed is not enough with high-speed targets of 5G usage scenarios [20]. Nevertheless, we show in this article why this 2 % rule does not apply to radar systems and when larger Doppler shift can be supported. The following usual assumption is also made in our study.

Assumption 3. *The radial speed* v *of the target is such that* $\frac{v}{c} \ll 1$.

The radar can process the OFDM signal as a pulse modulated waveform. The radar signal processing is then based on the ambiguity function analysis [21], [22]. This conventional radar approach does not require an OFDM signal with a cyclic prefix, contrary to an "OFDM approach", where the cyclic prefix provides *i*) an inter-delay-cell interference free signal in the radar system [23], *ii*) an inter-symbol interference free signal in the communication system [24]. We choose the OFDM approach to benefit from the cyclic prefix for both systems. The first step of the OFDM radar is then to demodulate the OFDM signal, as in the communication system.

The guard interval requirement allows for one tap per sub-carrier to demodulate the OFDM signal, as is already the case in OFDM communication systems. Either the delay $\tau(t)$ must be lower than τ_g, or the energy reflected by a target with delay larger than τ_g must be insignificant. The following assumption is then made.

Assumption 4. *The OFDM guard interval is correctly designed, i.e.,* $\tau_g \geq \tau(t)$ *and the window of the Fourier transform is correctly positioned, i.e.,* $\tau(t) \geq 0$.

The goal of the OFDM demodulation is to pick up the useful part of the signal, applying the fast Fourier transform, as would the communication system. Let us consider

the k-th OFDM symbol sampled at $t = \frac{jT}{n} + k(T+\tau_g) + \tau_g$, $j = 0, \cdots, n-1$. The digital base-band received signal is

$$y_k(j) = \frac{1}{\sqrt{n}} \sum_{i=0}^{n-1} a_{k,i} e^{2\imath\pi \frac{i}{T}\left(\frac{jT}{n}(1-\frac{2v}{c})-\tau_k\right)} e^{-2\imath\pi f_c\left(\tau_k + \frac{jT}{n}\frac{2v}{c}\right)} + b_k(j)\,, \tag{12}$$

which is given by (5) when $\tau_k = v = 0$. Using Assumptions 1 and 3, it becomes

$$y_k(j) = \frac{e^{\imath\phi_k}}{\sqrt{n}} \sum_{i=0}^{n-1} a_{k,i} e^{2\imath\pi \frac{ij}{n}} e^{-2\imath\pi \frac{i\tau_k}{T}} e^{-2\imath\pi \frac{j\nu T}{n}} + b_k(j)\,, \tag{13}$$

with $\phi_k = -2\pi f_c \tau_k$, and $\nu = f_c \frac{2v}{c}$ is the Doppler shift. Note that the Doppler ν experienced by the radar system is not the residual Doppler $\tilde{\nu}$ experienced by the communication system and $\nu \geq \tilde{\nu}$. The digital signal $y_k(j)$ is OFDM demodulated using the Fourier transform

$$\begin{aligned} Y_k(l) &= \frac{1}{\sqrt{n}} \sum_{j=0}^{n-1} y_k(j) e^{-2\imath\pi \frac{jl}{n}} \\ &= e^{\imath\phi_k} \sum_{i=0}^{n-1} a_{k,i} e^{-2\imath\pi \frac{i\tau_k}{T}} D_n(i-l-\nu T) + B_k(l)\,, \end{aligned} \tag{14}$$

where

$$D_n(u) = e^{\imath\pi u(1-\frac{1}{n})} \frac{\sin \pi u}{n \sin \frac{\pi}{n} u} \tag{15}$$

$\forall u \neq 0$ and $D_n(0) = 1$. If $u \ll n$, then $|D(u)|$ can be approximated by $|\operatorname{sinc} \pi u|$, with $\operatorname{sinc} u = \frac{\sin u}{u}$, which leads to the next assumption.

Assumption 5. *The sub-carrier number and the Doppler shift are such that $\nu T \ll n$.*

The samples $Y_k(l)$, $l = 0, \cdots, n-1$ and $k = 0, \cdots, m-1$, are the inputs used to get the delay-Doppler response with Fourier transforms and to detect the targets. These samples constitute a frame of m OFDM symbols. After the OFDM demodulation, the next step is to apply the filter to concentrate the energy of the received signal. In communication systems, the samples $Y_k(l)$ in (14) are the decision variables used to estimate the transmitted symbol $a_{k,l}$ with inter-carrier interference due to the Doppler shift; in radar systems, the samples $Y_k(l)$ are combined to detect the target parameters using a filter.

III. Radar filters

A. Conventional filters

With the matched filter, the digital delay-Doppler response is the processing of m OFDM symbols of n samples

$$\chi_{\text{MF}}(i,j) = \frac{1}{\sqrt{nm}} \sum_{l=0}^{n-1} \sum_{k=0}^{m-1} Y_k(l) \overline{a}_{k,l} e^{2\imath\pi \frac{il}{n}} e^{-2\imath\pi \frac{jk}{m}}\,, \tag{16}$$

where $\overline{a}_{k,l}$ is the complex conjugate of $a_{k,l}$. With negligible Doppler degradation, i.e., $\nu T \ll 1$, $D_n(u \neq 0) = 0$, and

$$\chi_{\text{MF}}(i,j) = \frac{1}{\sqrt{nm}} \sum_{l=0}^{n-1} \sum_{k=0}^{m-1} \Big(|a_{k,l}|^2 e^{-2\imath\pi \frac{l\tau_k}{T}} e^{2\imath\pi \frac{il}{n}} \times e^{-2\imath\pi \frac{jk}{m}} e^{\imath\phi_k} + B_k(l) \overline{a}_{k,l} e^{2\imath\pi \frac{il}{n}} e^{-2\imath\pi \frac{jk}{m}} \Big)\,. \tag{17}$$

With non-negligible Doppler, when Assumption 3 applies and with an adapted m value, we can show that the intensity of the delay-Doppler response is maximal for $j = m\left(1 + \frac{\tau_g}{T}\right)\nu T$, where $T + \tau_g$ is the pulse repetition time. The maximal delay-response is thus obtained for this $j = m\left(1 + \frac{\tau_g}{T}\right)\nu T$ Doppler cut, which is the new assumption used throughout this article.

Assumption 6. *The delay-response is analysed with a convenient Doppler cut, i.e., $m\left(1 + \frac{\tau_g}{T}\right)\nu T$.*

Therefore, we can focus on the delay axis to address the degradation of the delay response due to the Doppler shift. The delay response of the k-th OFDM symbol is reduced to

$$\begin{aligned} \chi_{\text{MF}}(i) = \frac{e^{\imath\phi_k}}{\sqrt{n}} &\sum_{l=0}^{n-1} |a_{k,l}|^2 e^{-2\imath\pi \frac{l\tau_k}{T}} e^{2\imath\pi \frac{il}{n}} \\ &+ \frac{1}{\sqrt{n}} \sum_{l=0}^{n-1} B_k(l) \overline{a}_{k,l} e^{-\imath\phi_k} e^{2\imath\pi \frac{il}{n}} \end{aligned} \tag{18}$$

Let us assume the target delay τ_k such that $\frac{n\tau_k}{T} = i_\tau$, then $|\chi_{\text{MF}}(i_\tau)|^2 = \max_i |\chi_{\text{MF}}(i)|^2$ with a proper noise level. The MF is the filter that maximises the SNR of the main lobe and this SNR becomes n times the input SNR. All these SNR values are clearly defined in Section IV. Note that with the subsequent delay-Doppler processing in (17), also called short time-long time processing, the total processing gain is not n but $n \times m$.

In practice, $\frac{n\tau_k}{T}$ is real and can be reduced neither to $\mathbb{N}$ nor $\mathbb{Z}$. Non-integer values lead to spectrum leakage that can be managed with a correctly chosen window [25]. To not weigh down the analysis, only integer cases are presented in this article, which is also called on-grid analysis. The analysis can be easily generalised in all cases by considering the window characteristics.

Assumption 7. *The analysis is conducted in the case where $\frac{n\tau_k}{T} \in \mathbb{N}$, which is equivalent to the general case with a well chosen window to overcome the spectral leakage.*

Another filter, a mismatched filter [9, § 4.10.3], is introduced for JRC systems to recover the channel transfer function, or the channel impulse response, regardless of the data [1]. With the ZF, the delay profile is

$$\chi_{\text{ZF}}(i) = \frac{1}{\sqrt{n}} \sum_{l=0}^{n-1} \frac{Y_k(l)}{a_{k,l}} e^{2\imath\pi \frac{il}{n}} \tag{19}$$

and with a negligible Doppler degradation it writes

$$\begin{aligned} \chi_{\text{ZF}}(i) = \frac{e^{\imath\phi_k}}{\sqrt{n}} &\sum_{l=0}^{n-1} e^{-2\imath\pi \frac{l\tau_k}{T}} e^{2\imath\pi \frac{il}{n}} \\ &+ \frac{1}{\sqrt{n}} \sum_{l=0}^{n-1} \frac{B_k(l)}{a_{k,l}} e^{2\imath\pi \frac{il}{n}}\,. \end{aligned} \tag{20}$$

The ZF exhibits the impulse response of the target at the price of a lower SNR in the main lobe, compared to the MF.

However, with low noise levels, i.e., $\sigma_b^2 \to 0$, the secondary lobes tend to zero with the ZF, contrary to the MF. Note that the ZF and the MF give the same delay response if the amplitudes of the symbols are equal, i.e., $|a_{k,l}| = |a_{k,i}|\ \forall i,l$. This is limited to communication systems with phase-shift keying and 4-quadrature amplitude modulation (QAM). In practice, larger orders of constellation are combined with OFDM to get a high communication bit-rate.

It is possible to combine the advantages of both ZF and MF filters using the well-known WF, which is another mismatched filter.

B. Wiener filter

The WF is widely used in multi-user communication systems. Among other applications, this filter is used for multi-carrier code division multiple access (MC-CDMA) systems to benefit from ZF and MF capabilities [6]. The Wiener radar filter is applied as in MC-CDMA receiver, i.e., in the frequency domain, to minimise the mean square error between the transmitted symbol $a_{k,l}$ and the one received on each sub-carrier [26]. The coefficients of the WF are then $\frac{\overline{a}_{k,l}}{|a_{k,l}|^2+\sigma_b^2}$, $\forall k \in [0,m)$ and $\forall l \in [0,n)$, while they are $\overline{a}_{k,l}$ and $\frac{1}{a_{k,l}}$ with MF and ZF, respectively. With the WF, the delay profile is

$$\chi_{\mathrm{WF}}(i) = \frac{1}{\sqrt{n}} \sum_{l=0}^{n-1} Y_k(l) \frac{\overline{a}_{k,l}}{|a_{k,l}|^2+\sigma_b^2} e^{2\imath\pi \frac{il}{n}} . \tag{21}$$

With a negligible Doppler degradation, the delay response becomes

$$\begin{aligned}\chi_{\mathrm{WF}}(i) = \frac{e^{\imath\phi_k}}{\sqrt{n}} \sum_{l=0}^{n-1} \frac{|a_{k,l}|^2}{|a_{k,l}|^2+\sigma_b^2} e^{-2\imath\pi \frac{l\tau_k}{T}} e^{2\imath\pi \frac{il}{n}} \\ + \frac{1}{\sqrt{n}} \sum_{l=0}^{n-1} B_k(l) \frac{\overline{a}_{k,l}}{|a_{k,l}|^2+\sigma_b^2} e^{2\imath\pi \frac{il}{n}} .\end{aligned} \tag{22}$$

A first comparison of the three filters can be done, based on (18), (20) and (22). With low noise levels, i.e., $\sigma_b^2 \to 0$, the WF behaves like the ZF, and with $\sigma_b^2 \gg |a_{k,l}|^2$, the WF behaves like the MF, with a multiplicative coefficient. The well-known trade-off property of the WF is recovered, between the SNR maximisation of the MF and the distortion rejection of the ZF [27, § 6.2].

We can now move on to the core part of this article: the effect of the Doppler shift on the delay profile of the OFDM radar, where this delay profile is modelled as an r.v.

IV. Delay response

We start with the general expression of the delay profile for all the three presented filters. To lighten the notation, ϕ_k is set to zero. Then,

$$\begin{aligned}\chi(i) &= \frac{1}{\sqrt{n}} \sum_{l=0}^{n-1} Y_k(l) c_{k,l} e^{2\imath\pi \frac{il}{n}} \\ &= \frac{1}{\sqrt{n}} \sum_{l=0}^{n-1} \sum_{j=0}^{n-1} a_{k,j} c_{k,l} e^{2\imath\pi \left(\frac{il}{n} - \frac{\tau_k j}{T}\right)} D_n(j-l-\nu T) \\ &\quad + \frac{1}{\sqrt{n}} \sum_{l=0}^{n-1} B_k(l) c_{k,l} e^{2\imath\pi \frac{il}{n}} ,\end{aligned} \tag{23}$$

where $c_{k,l} \in \{\overline{a_{k,l}}; \frac{\overline{a_{k,l}}}{|a_{k,l}|^2}; \frac{\overline{a_{k,l}}}{|a_{k,l}|^2+\sigma_b^2}\}$ is the filter coefficient for MF, ZF and WF, respectively.

In communication systems, the complex symbols $a_{k,l}$ are unknown to the receiver and they are considered as r.v. Contrary to the communication receiver, the mono-static radar receiver knows the complex symbols. However, and to go further, the moments of the delay profile (23) are studied and the following assumption is required.

Assumption 8. *The symbols $a_{k,l}$ are independent and identically distributed (i.i.d.) proper complex r.v. with zero mean, variance σ_a^2 and forth moment μ_a^4.*

The first moment derivation can now be done using Assumptions 2, 7 and 8

$$\begin{aligned}E[\chi(i)] &= \frac{1}{\sqrt{n}} \sigma_{ca}^2 D_n(-\nu T) \sum_{j=0}^{n-1} e^{2\imath\pi \left(\frac{ij}{n} - \frac{\tau_k j}{n}\right)} \\ &= \sqrt{n} \sigma_{ca}^2 D_n(-\nu T) \delta_{i, \frac{n\tau_k}{T}} ,\end{aligned} \tag{24}$$

where $\delta_{i,j}$ is the Kronecker delta function, and $\sigma_{ca}^2 = E[a_{k,j} c_{k,j}]$ is a function of $|a_{k,l}|^2$, a second moment. The signal energy is proportional to the main lobe $|E[\chi(i_\tau)]|$, which is $\sqrt{n}$ with the MF and when $\nu T = 0$, because all the Fourier transforms are normalised to be a unit transformation in our derivations. With Assumption 8, the signal power is σ_a^2 and the input SNR is $\frac{\sigma_a^2}{\sigma_b^2}$.

The first moment analysis is not enough to study the secondary lobes, which all equal zero in (24), for the three filters. This analysis does not allow to calculate the SNR of the delay profile, which is expected to be $n\frac{\sigma_a^2}{\sigma_b^2}$ with the matched filter. A higher moment analysis is required.

The second moment analysis is based on the expectation of the intensity of the delay profile, i.e., $E[|\chi(i)|^2]$. With

$$A_{j,l} = a_{k,j} c_{k,l} e^{2\imath\pi \left(\frac{il}{n} - \frac{\tau_k j}{T}\right)} D_n(j-l-\nu T) \tag{25}$$

and using Assumptions 2 and 8, the expectation of the intensity of the delay function is

$$\begin{aligned}E[|\chi(i)|^2] &= \frac{1}{n} \sum_{l=0}^{n-1} \sum_{j=0}^{n-1} \sum_{l'=0}^{n-1} \sum_{j'=0}^{n-1} E[A_{j,l} \overline{A_{j',l'}}] \\ &\quad + \frac{1}{n} \sum_{l=0}^{n-1} E[|B_k(l)|^2] E[|c_{k,l}|^2] \\ &= \frac{1}{n} \sum_{l=0}^{n-1} E[|A_{l,l}|^2] + \frac{1}{n} \sum_{l=0}^{n-1} \sum_{\substack{j=0 \\ j\neq l}}^{n-1} E[|A_{j,l}|^2] \\ &\quad + \frac{1}{n} \sum_{l=0}^{n-1} \sum_{\substack{j=0 \\ j\neq l}}^{n-1} E[A_{j,j} \overline{A_{l,l}}] + \sigma_b^2 \sigma_c^2 .\end{aligned} \tag{26}$$

All the other terms $E[A_{j,l}\overline{A_{j',l'}}]$, i.e., with the index set $\{j, l=j, j'\neq j, l' \notin \{l, j'\}\} \cup \{j, l=j, j'=j, l'\neq l\} \cup \{j, l\neq j, j', l'\neq l\} \cup \{j, l, j'\neq j, l'=l\}$, are equal to zero in (26) because

i) $\{a_{k,l}\}_{l=0,\cdots,n-1}$ are zero mean, i.i.d. r.v.;
ii) $\{c_{k,l}\}_{l=0,\cdots,n-1}$ are zero mean, i.i.d. r.v.;
iii) $a_{k,l}$ and $c_{k,l'}$ are independent $\forall l \neq l'$.

The first results can now be stated, using the notations $E[|a_{k,j}c_{k,j}|^2] = \mu_{ca}^4$ and $E[|c_{k,j}|^2] = \sigma_c^2$.

Proposition 9. *The expectation of the intensity of the main lobe, at $i = i_\tau$, is*

$$E[|\chi(i_\tau)|^2] = \left(\mu_{ca}^4 + (n-1)\sigma_{ca}^4\right)\operatorname{sinc}^2 \pi\nu T + \sigma_c^2\sigma_a^2(1 - \operatorname{sinc}^2 \pi\nu T) + \sigma_c^2\sigma_b^2 \,.$$

Proof. See Appendix A. □

Proposition 9 gives a simple expression of the main lobe intensity. With a large n, i.e., with a large OFDM symbol size and high number of sub-carriers, the expectation of the main lobe intensity is approximated by $n\sigma_{ca}^4 \operatorname{sinc}^2 \pi\nu T$, which is $|E[\chi(i_\tau)]|^2$ given by the first moment analysis. The first moment analysis of the main lobe is reasonably enough in this case of a large OFDM symbol size. For all OFDM symbol sizes, the second moment expression is required and it is linked to the first one by

$$E[|\chi(i_\tau)|^2] = |E[\chi(i_\tau)]|^2 + (\mu_{ca}^4 - \sigma_{ca}^4)\operatorname{sinc}^2 \pi\nu T + \sigma_c^2\sigma_a^2(1 - \operatorname{sinc}^2 \pi\nu T) + \sigma_c^2\sigma_b^2 \,. \quad (27)$$

It is interesting to note that, in the expression of $E[|\chi(i_\tau)|^2]$, only the $|E[\chi(i_\tau)]|^2$ term depends on n. The noise contribution in (27) is $\sigma_c^2\sigma_b^2$, the SNR of the main lobe with MF and $\nu T = 0$ is then $n\frac{\sigma_a^2}{\sigma_b^2}$, n times the input SNR as expected.

The next step is to find the properties of the secondary lobes.

Proposition 10. *The secondary lobes intensity is asymptotically an exponential r.v. with parameter λ such that*

$$\frac{1}{\lambda} = E[|\chi(i_\tau)|^2] - n\sigma_{ca}^4 \operatorname{sinc}^2 \pi\nu T \,.$$

Proof. See Appendix B. □

Using Propositions 9 and 10, the expectation of the secondary lobes intensity does not depend on n. When n increases, the main lobe intensity increases, but the mean secondary lobes intensity remains unchanged. One obtains that the mean distance between the main lobe and the secondary ones is $n\sigma_{ca}^4 \operatorname{sinc}^2 \pi\nu T$, which increases with n. This distance is then zero when the Doppler shift is a multiple of the sub-carrier spacing.

V. Application to PSLR, ISLR and SINR

A. Radar metrics

Instead of the distance, two ratios are used to characterise the delay profile and to reduce it to one parameter. These ratios are the PSLR

$$\gamma_{\text{PSLR}} = E\left[\frac{|\chi(i_\tau)|^2}{\max\limits_{i\neq i_\tau}|\chi(i)|^2}\right] \quad (28)$$

and the ISLR

$$\gamma_{\text{ISLR}} = E\left[\frac{|\chi(i_\tau)|^2}{\sum\limits_{i\neq i_\tau}|\chi(i)|^2}\right] . \quad (29)$$

These metrics can be linked to the performance of target detectors, like the adaptive threshold detector [9]. Both PSLR and ISLR depend on the energy of the main lobe. In our model, the main lobe size equals one because the sampling frequency is the nominal OFDM one, and the analysis is done under Assumption 7. This energy is then reduced to $|\chi(i_\tau)|^2$. With an anti-leakage window, the main lobe size is larger and this has to be considered in the PSLR and ISLR definition. We continue the derivations under Assumption 7.

Proposition 11. *The PSLR is*

$$\gamma_{PSLR} \approx \frac{1}{H_{n-1}} + \frac{\frac{n}{H_{n-1}}}{\frac{\mu_{ca}^4}{\sigma_{ca}^4} - 1 + \frac{\sigma_c^2}{\sigma_{ca}^4}\frac{\sigma_a^2(1-\operatorname{sinc}^2 \pi\nu T)+\sigma_b^2}{\operatorname{sinc}^2 \pi\nu T}} \,,$$

with H_n the nth harmonic number.

Proof. See Appendix C. □

For a constant noise and fixed modulation parameters, and with a large number n of sub-carriers, the PSLR is proportional to $\frac{n}{H_{n-1}}$. The explanation is as follows: *i)* the intensity of the main lobe is proportional to n; *ii)* the mean secondary lobes intensity does not depend on n, however the probability of having larger secondary lobes increases with n. Therefore, the largest secondary lobe intensity depends on n and it is proportional to H_{n-1}. The ratio between the intensity of the main lobe and the intensity of the largest secondary lobe gives the asymptotic result, i.e., when n is large.

Proposition 12. *The ISLR is*

$$\gamma_{ISLR} \approx \frac{1}{n-1} + \frac{1 + \frac{1}{n-1}}{\frac{\mu_{ca}^4}{\sigma_{ca}^4} - 1 + \frac{\sigma_c^2}{\sigma_{ca}^4}\frac{\sigma_a^2(1-\operatorname{sinc}^2 \pi\nu T)+\sigma_b^2}{\operatorname{sinc}^2 \pi\nu T}} \,.$$

Proof. See Appendix D. □

The PSLR and ISLR depend on each other. The ISLR used here can be obtained from the PSLR with the equality

$$(n-1)\gamma_{\text{ISLR}} = H_{n-1}\gamma_{\text{PSLR}} \,, \quad (30)$$

which is based on Propositions 11 and 12.

Propositions 11 and 12 exhibit the characteristics of the three filters through $\frac{\mu_{ca}^4}{\sigma_{ca}^4}$ and $\frac{\sigma_c^2}{\sigma_{ca}^4}$.

B. MF, ZF and WF comparison

The three filters are characterised by the filter coefficients c_k and the parameters μ_{ca}^4, σ_{ca}^2 and σ_c^2, with expressions summarised in Table I. Note that the filters are applied in the frequency domain with only one coefficient c_k, a multiplying factor, per subcarrier k, as in the OFDM communication system [26]. The differences between the three filters are given by the expression of c_k, which needs

Table I
MODULATION PARAMETERS.

	MF	ZF	WF
c_k	$\overline{a_k}$	$\frac{\overline{a_k}}{\lvert a_k\rvert^2}$	$\frac{\overline{a_k}}{\lvert a_k\rvert^2+\sigma_b^2}$
μ_{ca}^4	μ_a^4	1	$E\left[\frac{\lvert a_{k,i}\rvert^4}{(\lvert a_{k,i}\rvert^2+\sigma_b^2)^2}\right]$
σ_{ca}^2	σ_a^2	1	$E\left[\frac{\lvert a_{k,i}\rvert^2}{\lvert a_{k,i}\rvert^2+\sigma_b^2}\right]$
σ_c^2	σ_a^2	$E\left[\frac{1}{\lvert a_{k,i}\rvert^2}\right]$	$E\left[\frac{\lvert a_{k,i}\rvert^2}{(\lvert a_{k,i}\rvert^2+\sigma_b^2)^2}\right]$

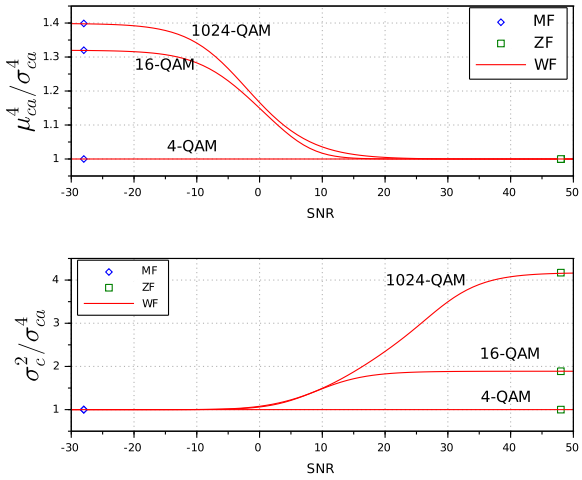

Figure 1. Normalised delay response parameters versus input SNR in dB, for $\{4, 16, 1024\}$-QAM.

the knowledge of the transmitted symbol a_k for the three filters, and the knowledge of the noise power σ_b^2 for the WF. The parameters characterise the constellation size and shape. Contrary to the MF and ZF, the modulation parameters with the WF depend on the noise level σ_b^2. Fig. 1 plots $\frac{\mu_{ca}^4}{\sigma_{ca}^4}$ and $\frac{\sigma_c^2}{\sigma_{ca}^4}$ versus the input SNR $\frac{\sigma_a^2}{\sigma_b^2}$ for the WF, and for three QAM. In this results, the power of the constellations is normalised such as $\sigma_a^2 = 1$. As the MF and ZF do not depend on the input SNR, only one point per modulation is plotted for both $\frac{\mu_{ca}^4}{\sigma_{ca}^4}$ and $\frac{\sigma_c^2}{\sigma_{ca}^4}$ parameters, and it is positioned where the convergence with the WF occurs. Furthermore, $\frac{\mu_{ca}^4}{\sigma_{ca}^4}$ does not depend on the constellation size for the ZF, but it depends on the constellation size for the MF. The opposite is observed with $\frac{\sigma_c^2}{\sigma_{ca}^4}$: it does not depend on the constellation size for MF as it would with the ZF. As expected, the modulation parameters with the WF vary between the MF and the ZF, with a dependency with the size of the constellation. The WF becomes the MF when the input SNR approaches zero, i.e., the noise approaches infinity, and it becomes the ZF when the input SNR goes to infinity, i.e., the noise approaches zero.

C. Robustness of OFDM communication

To compare radar and communication systems, we provide a new formulation of the SINR (7) using the derivation developed for the analysis of the delay function.

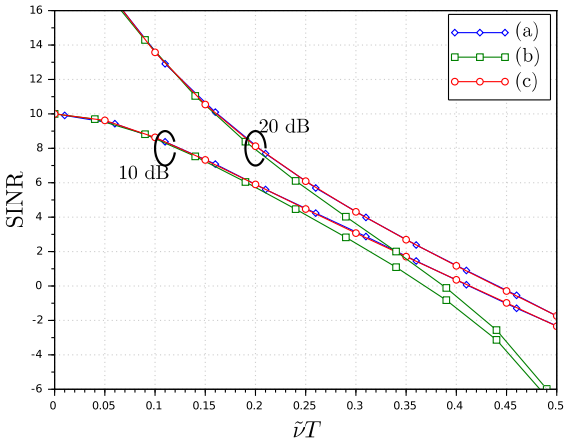

Figure 2. OFDM SINR, (a) simulation, (b) from (7), (c) Proposition 13, in dB versus $\tilde{\nu}T$, with $n = 2^8$, 16-QAM, input SNR of 10 and 20 dB.

The SINR is defined by the ratio on the mean value of the signals at the output of the demodulated OFDM symbol

$$\gamma_{\text{SINR}} = \frac{\frac{1}{n}\sum_l S_l}{\frac{1}{n}\sum_l I_l}, \tag{31}$$

where S_l is the useful signal power and I_l is the power of the interference plus noise on sub-carrier l (14). We recall that the Doppler experienced by the communication system is the residual Doppler $\tilde{\nu}$ and not the Doppler ν, because of the synchronisation process in the communication system that reduces ν to $\tilde{\nu}$.

Proposition 13. *The SINR is*

$$\gamma_{SINR} = \frac{\text{sinc}^2\,\pi\tilde{\nu}T}{1 - \text{sinc}^2\,\pi\tilde{\nu}T + \frac{\sigma_b^2}{\sigma_a^2}}.$$

Proof. See Appendix E. □

Proposition 13 provides an exact expression of the SINR and its validity is now numerically evaluated. Fig. 2 compares (7), curve (b), and Proposition 13, curve (c), in the case where $n = 2^8$. The modulation tested by simulation is the 16-QAM. Both curves (b) and (c) are compared to the SINR (31) obtained by simulation, curve (a). The simulation values, curve (a), are superimposed to the results obtained with Proposition 13, curve (c). This superimposition shows the accuracy of the proposed analytical approach for all the residual Doppler $\tilde{\nu}T$ and the input SNR, whereas the gap between the curves (a) and (b), which is obtained with the approximation (7), crumbles when $\tilde{\nu}T \geq 0.3$.

The SINR is also linked to the PSLR and ISLR approximations, which constitutes the next proposition, and which is the interest of Proposition 13.

Proposition 14. *Under the same Doppler and residual Doppler shift, the PSLR is a function of the SINR with*

$$\gamma_{PSLR} \approx \frac{1}{H_{n-1}} + \frac{\frac{n}{H_{n-1}}}{\frac{\mu_{ca}^4}{\sigma_{ca}^4} - 1 + \frac{\sigma_c^2\sigma_a^2}{\sigma_{ca}^4}\frac{1}{\gamma_{SINR}}}.$$

Proof. The result is obtained by combining Proposition 11 and 13 with $\nu = \tilde{\nu}$. □

Proposition 14 shows the link between the PSLR and the SINR. The radar performance is then linked to the communication one. Obviously, the PSLR is a positive, increasing and concave function of the SINR. The remarkable result is that this link does not depend on the Doppler shift, nor the sub-carrier spacing[2]. It depends only on the number n of sub-carriers and on the parameters of the constellations. Another interesting result is that the radar system benefits from the number n of sub-carriers more than the communication system does, as the PSLR increases with n at a given SINR. However, Proposition 14 is quite limited, as $\nu \neq \tilde{\nu}$ in practice. Nevertheless, it is used to show how both radar and communication systems are robust to their own Doppler shift.

A similar proposition can be simply derived for the ISLR using (30).

VI. Extension to non-full OFDM signal

With the scenario presented in Section II, one JRC platform can use all the sub-carriers of the OFDM symbols, but only one platform can transmit on a space-time-frequency resource at a time to ensure interference free communications and interference free radar detection. To increase the communication and radar flexibility, multiple transmissions should be possible at the same space-time-frequency resource in a given area. The interference is then mitigated in the waveform domain [14]. Random sparse OFDM symbols can then be used, where a random sequence of active sub-carriers is assigned to each JRC platform in the given area. To perform interference free systems, the sequences have to be managed by the network in a centralised or in an ad-hoc manner.

The transmitted symbols are defined in $\mathbb{C}$ instead of $\mathbb{C}\backslash\{0\}$ to take into account the empty sub-carriers, which are the inactive sub-carriers. We model the random set of active and inactive sub-carriers with a Bernoulli r.v. with parameter p. To simplify the analysis, the symbol $a_{k,i}$ transmitted on the sub-carrier i of the k-th OFDM symbol becomes $p_{k,i}a_{k,i}$, with $a_{k,l} \in \mathbb{C}\backslash\{0\}$, $p_{k,i} \in \{0,1\}$ and $E[p_{k,i}] = p$ for all k and i. With this model, the delay profile (23) becomes

$$\chi(i) = \frac{1}{\sqrt{n}} \sum_{l=0}^{n-1}\sum_{j=0}^{n-1} p_{k,j}a_{k,j}p_{k,l}c_{k,l}e^{2\imath\pi\left(\frac{il}{n} - \frac{\tau_k j}{T}\right)} \qquad (32)$$

[2]This analysis can be misleading, because the parameter is the sub-carrier spacing $\frac{1}{T}$ and the relative Doppler νT does not depend on n, in our approach. If the parameter had been the bandwidth $W = \frac{n}{T}$, the relative Doppler would have been $\frac{\nu n}{W}$, and then it would have depended on the number n of sub-carriers. However, we choose to work with fixed OFDM symbol time duration.

$$\times D_n(j - l - \nu T) + \frac{1}{\sqrt{n}}\sum_{l=0}^{n-1} B_k(l)p_{k,l}c_{k,l}e^{2\imath\pi\frac{il}{n}}.$$

Using (32) and Proposition 11, we can now derive the last proposition.

Proposition 15. *The PSLR with the sparse OFDM signal is*

$$\gamma_{PSLR} \approx \frac{1}{H_{n-1}} + \frac{\frac{n}{H_{n-1}}}{\frac{\mu_{ca}^4}{p\sigma_{ca}^4} - 1 + \frac{\sigma_c^2}{\sigma_{ca}^4}\frac{\sigma_a^2(1-\text{sinc}^2\,\pi\nu T) + \frac{\sigma_b^2}{p}}{\text{sinc}^2\,\pi\nu T}}.$$

Proof. See Appendix F. □

Proposition 15 shows that the PSLR is an increasing function of p and n, but in a different way. The PSLR with the couple of the number of sub-carriers and the ratio of activity (n,p) with $p < 1$ is not the PSLR with $(np, 1)$. It can also be proved that the PSLR with (n,p) and $p < 1$ is lower than the PSLR with $(np, 1)$, when νT is not to high, i.e., $\nu T < 0.4$.

VII. Simulation results

The transmitted OFDM signal uses n sub-carriers with QAM, which are all active, $p = 1$. All Assumptions 1 to 8 are taken into account in the simulated radar-communication system. The simulation results are based on (23), the exact expression of the output filters. None of the results depend on the chosen value i_τ, which is arbitrarily set to zero. The input SNR is $\frac{\sigma_a^2}{\sigma_b^2}$ and the power of the constellations is normalised to 1. Some numerical values of the constellation parameters are given in [28]. The number of considered OFDM symbols in a frame is 1, since there is no slow time radar signal processing in our analysis. The results can be extended to an operating delay-Doppler radar system by simply multiplying all the gains by m to take into account the slow time processing. From Figure 4 to Figure 9, the solid line curves are for the analytical results and the marks are for the simulation results.

Fig. 3 gives the histogram of the secondary lobes, i.e., $|\chi(i \neq i_\tau)|^2$, of the three filters with $n = 2^{13}$, $\nu T = 0.1$, a 16-QAM and with an input SNR of 10 dB. The empirical distributions, obtained from the square of the amplitude of (23), for $i \neq i_\tau$ and for one OFDM symbol, are compared to the probability density functions obtained with Proposition 10. The figure confirms the accuracy of our analytical derivations.

The PSLR versus the input SNR is presented in Fig. 4. The simulation results are given by (28) and the analytical ones are obtained with Proposition 11. The curves confirm

1) The accuracy of our analytical developments;
2) The behaviour of the WF, between the MF and the ZF.

For a null Doppler, the WF tends to the MF at low SNR and outperforms the ZF, whereas it tends to the ZF at high SNR and outperforms the MF. However, for a Doppler value of 40 % of the sub-carrier spacing and for a large

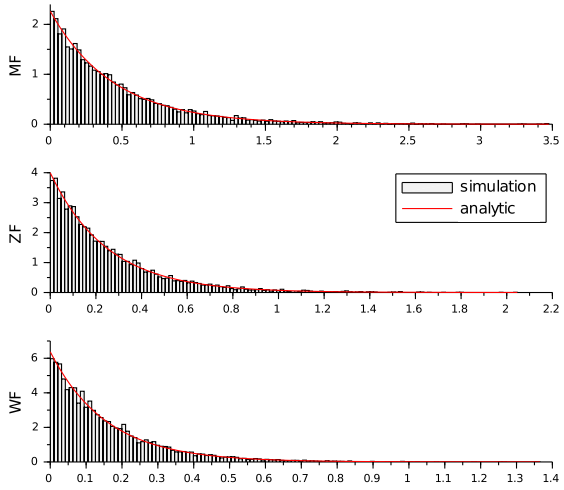

Figure 3. Secondary lobe distributions with $\sigma_a^2/\sigma_b^2 = 10$ dB, $n = 2^{13}$, $\nu T = 0.1$, 16-QAM.

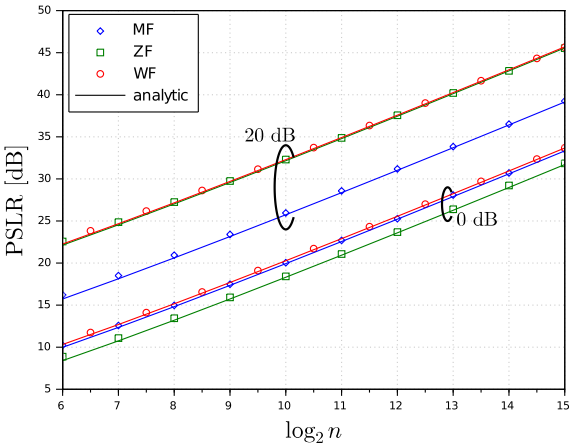

Figure 6. PSLR in dB versus n with 16-QAM, $\nu T = 0.1$, and two input SNR $\{0, 20\}$ dB.

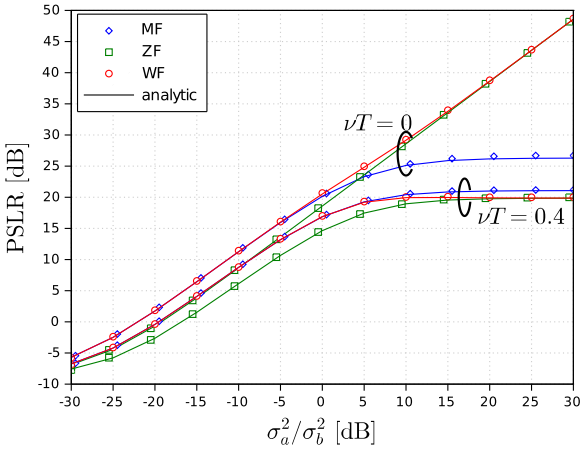

Figure 4. PSLR in dB versus the input SNR in dB with $n = 2^{10}$, $\nu T \in \{0; 0.4\}$, 16-QAM.

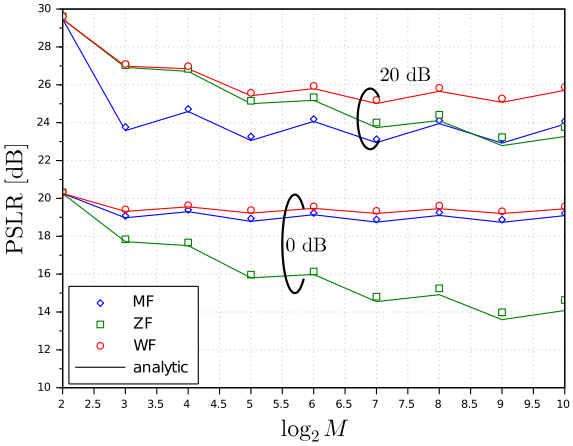

Figure 7. PSLR in dB versus the constellation size M with $n = 2^{10}$, $\nu T = 0.2$ and two input SNR $\{0, 20\}$ dB.

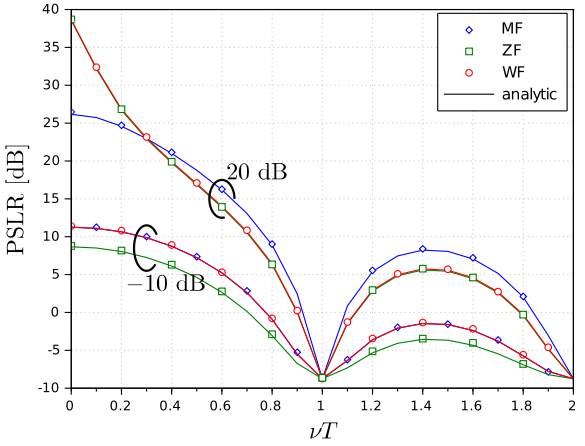

Figure 5. PSLR in dB versus νT with $\sigma_a^2/\sigma_b^2 \in \{-10, 20\}$ dB, $n = 2^{10}$, 16-QAM.

input SNR, the MF still outperforms the WF. This is highlighted in Fig. 5 where the PSLR is plotted versus the Doppler νT. For a large input SNR, 20 dB here, the PSLR of the WF and ZF are superimposed, but they remain up to 3 dB below the PSLR of the MF for $\nu T > 0.3$. In this case, a large input SNR and Doppler, the maximisation of the SNR of the main lobe becomes decisive to improve the PSLR. Hence, the MF is the only best filter in this case. As exhibited in Fig. 5, the ZF and WF PSLR are sensitive to the Doppler at a high SNR regime, i.e., 20 dB. The PSLR crashes and loses more than 10 dB with a 0.2 increase in νT. In contrast in a lower SNR regime, the ZF and WF PSLR are robust and can support Doppler shifts up to 20 % of sub-carrier spacing with less than 1 dB of degradation. Contrary to WF and ZF, the MF is robust in any SNR regime. In a low SNR regime, -10 dB, the MF and WF PSLR are superimposed and outperform the ZF one.

The next two figures show the PSLR versus the number n of sub-carriers and the size M of the constellations, i.e., the M-QAM. Fig. 6 exhibits a quasi-linear dependence of the PSLR on n, with a logarithmic axis. The slope of the curves is around $\frac{5}{2}$, which means that the dependence is sub-linear with a linear power-law coefficient around 0.8. Fig. 7 shows a counter-intuitive result with a high input SNR: the WF deviates from the ZF when the constellation size increases. The explanation is that the high SNR regime depends on the size of the constellation, and 20 dB is not high enough for a 64-QAM, contrary to smaller constellation sizes. The shape of the curves is saw-tooth, because the constellations are square when M is a power of even numbers, and they are rectangular when M is a power of odd numbers. The differences between the analysis and simulation, which come from Jensen's inequality in Proposition 11 and are less than 0.1 dB as in other figures, are more visible in this Fig. 7, because of the close up into the y-axis.

The same comparisons and relative results, not presented here, are obtained with the ISLR, which is deduced from the PSLR using (30). The accuracy of the last results, given by Proposition 14 and Proposition 15, are also verified in all the presented cases. The Doppler independence of the PSLR from the SINR is verified. The Doppler shift affects the radar system performance as much as the residual Doppler shift affects the communication system performance, when the Doppler is relative to the carrier spacing. A higher SNR means that the radar system can detect farther targets or targets with lower RCS.

VIII. JRC system design

The JRC requirements can be given as the SINR and PSLR measures, for the communication and radar parts, respectively. Feasibility regions can be expressed as a function of the input SNR and the relative Doppler νT and $\tilde{\nu} T$ supported by the JRC system. With Propositions 11 and 13, the bound of the feasibility region is derived through the lowest SNR the system can handle at a given Doppler shift.

The two last figures, Fig. 8 and 9, give the SNR-Doppler couples that fulfil the JRC system requirements. In Fig. 8, the Doppler $\tilde{\nu} T$ is the relative residual Doppler not corrected by the synchronisation process. For example, a minimal SNR of 12 dB is required to ensure a SINR of 5 dB at a residual Doppler shift of 0.25. If a 2 % of the sub-carrier spacing ensures a negligible SNR degradation and enough margin of safety for operating systems, more residual Doppler can be supported at low SINR requirements, i.e., when the communication system uses low orders of modulation. The figure also exhibits the maximal residual Doppler supported, but at a price of a noiseless transmission, i.e., infinite input SNR. In Fig. 9, the Doppler νT is the one seen by the radar system. Only few results of simulations are provided to not clutter this figure. Three particular PSLR values are chosen to exhibit the filter behaviours. At low PSLR requirements, huge Doppler shifts can be supported, up to 0.7 at a PSLR of 10 dB. At high PSLR requirements, i.e., 30 dB, the

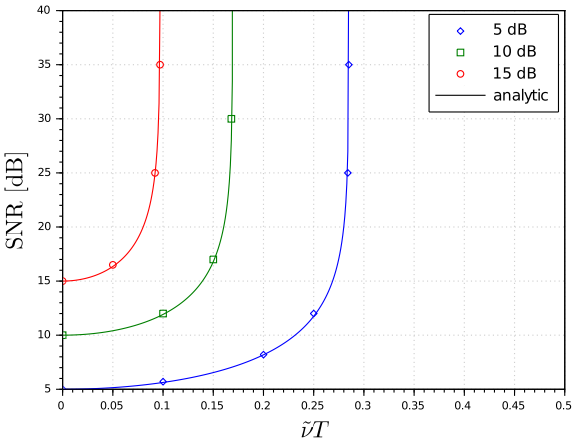

Figure 8. Required input SNR in dB versus $\tilde{\nu} T$ to reach 4 SINR values in dB, $\{5, 10, 15\}$.

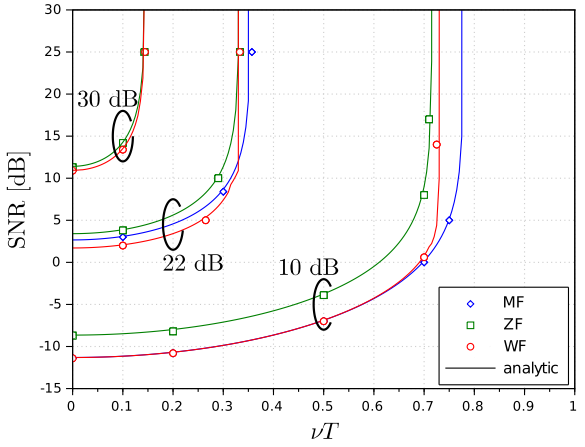

Figure 9. Required input SNR in dB versus νT to reach 4 PSLR values in dB, $\{10, 22, 30\}$, $n = 2^{10}$, 16-QAM.

MF does not operate and it needs a larger sub-carriers number. Note that the ZF needs higher SNR than the MF at low and medium PSLR requirements. This figure also demonstrates the capabilities of the WF compared to the MF and ZF. In a wide range of SNR-Doppler couples, the WF outperforms the MF and ZF. It needs lower SNR at a given Doppler to satisfy the PSLR requirement.

IX. Conclusion

This article has quantified the Doppler robustness of the OFDM waveform in the JRC context. The dual communication and radar system uses a single OFDM signal to perform communication and radar applications at the same time. Both systems have been studied within the same analytical framework, leading to an expression that links the radar performance to the communication one. The radar system benefits from the proposed Wiener filter, and the configurations where this filter outperforms the other

ones are outlined. All the results have been conducted in an interference free scenario for both systems, using an orthogonal transmission in space-time-frequency domain. Further works will be provided in the case of interference scenarios and non orthogonal multiple access systems.

Appendix A
Proof of Proposition 9

The main lobe intensity is obtained for $i_\tau = \frac{n\tau_k}{T}$. The three terms in (26) have to be calculated

$$E[|A_{j,j}|^2] = E[|a_{k,j}c_{k,j}|^2]|D_n(\nu T)|^2\,, \tag{33}$$

and for all $j \neq l$

$$\begin{aligned} E[|A_{j,l}|^2] &= E[|a_{k,j}c_{k,l}|^2]D_n(j-l-\nu T)^2 \\ &= E[|a_{k,j}|^2]E[|c_{k,l}|^2]|D_n(j-l-\nu T)|^2 \end{aligned} \tag{34}$$

and

$$\begin{aligned} &E[A_{j,j}\overline{A_{l,l}}] \\ &\quad= E[a_{k,j}c_{k,j}]E[\overline{a_{k,l}c_{k,l}}]e^{2\imath\frac{\pi}{n}\left(i_\tau-\frac{\tau_k n}{T}\right)(j-l)}|D_n(\nu T)|^2 \\ &\quad= E[a_{k,j}c_{k,j}]E[\overline{a_{k,l}c_{k,l}}]|D_n(\nu T)|^2\,. \end{aligned} \tag{35}$$

Using Assumption 5, and with (33), (34) (35) and (26), the expectation of the main lobe intensity is

$$\begin{aligned} E[|\chi(i_\tau)|^2] = &\left(\mu_{ca}^4 + (n-1)\sigma_{ca}^4\right)\operatorname{sinc}^2\pi\nu T + \sigma_c^2\sigma_a^2 g_n(\nu T) \\ &+ \sigma_c^2\sigma_b^2\,, \end{aligned} \tag{36}$$

where

$$\begin{aligned} g_n(x) &= \frac{1}{n}\sum_{j=0}^{n-1}\sum_{\substack{l=0\\l\neq j}}^{n-1}\frac{\sin^2\pi x}{n^2\sin^2\frac{\pi}{n}(j-l-x)} \\ &= \sum_{j=1}^{n-1}\frac{n-j}{n}\left(\frac{\sin^2\pi x}{n^2\sin^2\frac{\pi}{n}(j-x)} + \frac{\sin^2\pi x}{n^2\sin^2\frac{\pi}{n}(j+x)}\right) \end{aligned} \tag{37}$$

for all $x \in \mathbb{R}_+\backslash\mathbb{N}$, and for the all the integers y where the function is not defined, $g_n(y) = \lim_{x\to y} g_n(x)$. A simpler expression of this function g_n can be given. We then need the following proposition to finish the proof of Proposition 9.

Proposition 16. *For all $x \in \mathbb{R}$*

$$g_n(x) = 1 - |D_n(x)|^2\,.$$

Proof. We use the complete summation to obtain the result

$$\begin{aligned} g_n(x) + |D_n(x)|^2 &= \frac{1}{n^3}\sum_{j=0}^{n-1}\sum_{l=0}^{n-1}\frac{\sin^2\pi x}{\sin^2\frac{\pi}{n}(j-l-x)} \\ &= \frac{1}{n^3}\sum_{j=0}^{n-1}\sum_{l=0}^{n-1}\left|\sum_{k=0}^{n-1}e^{2\imath\frac{\pi}{n}(j-l-x)k}\right|^2 \\ &= \frac{1}{n^3}\sum_{k=0}^{n-1}\sum_{i=0}^{n-1}e^{-2\imath\frac{\pi}{n}x(k-i)}\left|\sum_{j=0}^{n-1}e^{2\imath\frac{\pi}{n}j(k-i)}\right|^2 \\ &= \frac{1}{n}\sum_{k=0}^{n-1}\sum_{i=0}^{n-1}e^{-2\imath\frac{\pi}{n}x(k-i)}\delta_{k,i} \\ &= 1\,, \end{aligned} \tag{38}$$

where $\delta_{k,i}$ is the Kronecker delta function. □

Proposition 16 is then used in (36) to finish the proof of Proposition 9. With Assumption 5, the sinc function can be used instead of the ratio of sinus functions.

Appendix B
Proof of Proposition 10

The expectation of the secondary lobes intensity is $E[|\chi(i)|^2]$ with $i \neq i_\tau$. The three terms of (26), already calculated when $i = i_\tau$ in the proof of Proposition (9), have to be calculated when $i \neq i_\tau$. Only $E[A_{j,j}\overline{A_{l,l}}]$ differs and it equals zero when $i \neq i_\tau$. As the reciprocal of the parameter λ of an exponential r.v. is its expectation, the mathematical expression of the proposition is then proved. It remains to obtain that the secondary lobes are an exponential r.v. To simplify the analysis, let $\tau_k = 0$. Therefore, (23) becomes

$$\begin{aligned} \sqrt{n}\chi(i) = &\sum_{l=1}^{n-1}\sum_{j=0}^{n-1}a_{k,j}c_{k,l}e^{2\imath\pi\frac{il}{n}}D_n(j-l-\nu T) \\ &+ \sum_{l=0}^{n-1}B_k(l)c_{k,l}e^{2\imath\pi\frac{il}{n}}\,. \end{aligned} \tag{39}$$

The second term in (39) is an independent sum of n complex Gaussian r.v. This term is then complex Gaussian. The first term is composed of n^2 independent r.v. $a_{k,j}c_{k,l}e^{2\imath\pi\frac{il}{n}}D_n(j-l-\nu T)$ uniformly dominated

$$|a_{k,j}c_{k,l}e^{2\imath\pi\frac{il}{n}}D_n(j-l-\nu T)| \leq \max|a_{k,j}|\max|c_{k,l}|\,, \tag{40}$$

where the maximum are evaluated over all the points of the constellation. The variance of the r.v. of the first term of (39) is

$$\begin{cases} \sigma_a^2\sigma_c^2|D_n(j-l-\nu T)|^2, & \forall j \neq l, \\ (\mu_{ca}^4 - \sigma_{ca}^4)|D_n(-\nu T)|^2, & \forall j = l, \end{cases} \tag{41}$$

and the sum of these n^2 variances goes to infinity with n. Under the conditions of uniform bound of the n^2 r.v. and unbounded sum of the n^2 variances, the Lindeberg's theorem implies that the first term converges also to a complex Gaussian r.v. [29, § 7.3.1]. Then, $\sqrt{n}\chi(i)$ is the sum of two Gaussian r.v. and converges to a complex Gaussian r.v. The secondary lobes $|\chi(i)|^2$ are asymptotically a chi-squared r.v. with two degrees of freedom, i.e., an exponential r.v.

Appendix C
Proof of Proposition 11

Firstly, using the first order of the Taylor expansion, or the Jensen's inequality, the expectation of a ratio in (28) is approximated by the ratio of the expectations

$$E\left[\frac{|\chi(i_\tau)|^2}{\max\limits_{i\neq i_\tau}|\chi(i)|^2}\right] \approx \frac{E[|\chi(i_\tau)|^2]}{E[\max\limits_{i\neq i_\tau}|\chi(i)|^2]}. \tag{42}$$

Secondly, the expectation in the denominator in (42), which is the expectation of the maximal value of $n-1$ r.v. $\{|\chi(i)|^2\}_{i\neq i_\tau}$, is obtained using the $n-1$-th order statistic, i.e., the largest order statistic. Then, with F the cumulative distribution function of $|\chi(i)|^2$, and with Proposition 10,

$$\begin{aligned} E[\max_{i\neq i_\tau}|\chi(i)|^2] &= \int_0^\infty \frac{\partial F(x)^{n-1}}{\partial x} x dx \\ &= \int_0^\infty (n-1)\lambda e^{-\lambda x}(1-e^{-\lambda x})^{n-2} x dx \\ &= \frac{1}{\lambda}\sum_{k=1}^{n-1}\frac{(-1)^{k+1}}{k}\binom{n-1}{k} \\ &= \frac{1}{\lambda}\sum_{k=1}^{n-1}\frac{1}{k}, \end{aligned} \tag{43}$$

where the last equality can be obtained by mathematical induction. The combination of (43), (28) and Propositions 9 and 10 ends the proof.

Appendix D
Proof of Proposition 12

The Jensen's inequality is also used and

$$E\big[\sum_{i\neq i_\tau}|\chi(i)|^2\big] = (n-1)E[|\chi(i\neq i_\tau)|^2]\,. \tag{44}$$

The proof is ended using Propositions 9 and 10.

Appendix E
Proof of Proposition 13

Using (14),

$$\begin{aligned} S_l &= E\left[\left|e^{\imath\pi_k}a_{k,l}e^{-2\imath\pi\frac{l\tau_k}{T}}D_n(-\tilde{\nu}T)\right|^2\right] \\ &= \sigma_a^2|D_n(\tilde{\nu}T)|^2 \end{aligned} \tag{45}$$

and

$$\begin{aligned} I_l &= E\left[\left|e^{\imath\pi_k}\sum_{\substack{i=0\\ i\neq l}}^{n-1}a_{k,l}e^{-2\imath\pi\frac{i\tau_k}{T}}D_n(i-l-\tilde{\nu}T)+B_k(i)\right|^2\right] \\ &= \sigma_a^2\sum_{\substack{i=0\\ i\neq l}}^{n-1}|D_n(i-l-\tilde{\nu}T)|^2+\sigma_b^2\,. \end{aligned} \tag{46}$$

Then,

$$\gamma_{\text{SINR}} = \frac{|D_n(\tilde{\nu}T)|^2}{\sum_{l=0}^{n-1}\sum_{\substack{i=0\\ i\neq l}}^{n-1}|D_n(i-l-\tilde{\nu}T)|^2+\frac{\sigma_b^2}{\sigma_a^2}}\,. \tag{47}$$

The proof is concluded with Proposition 16 in Appendix A.

Appendix F
Proof of Proposition 15

With (32), the expectations needed to calculate the average intensity of the lobes are

$$E[|p_{k,j}a_{k,j}p_{k,j}c_{k,j}|^2] = pE[|a_{k,j}c_{k,j}|^2] = p\mu_{ca}^4\,, \tag{48}$$
$$E[|p_{k,j}a_{k,j}|^2] = pE[|a_{k,j}|^2] = p\sigma_a^2\,, \tag{49}$$
$$E[|p_{k,j}c_{k,j}|^2] = pE[|c_{k,j}|^2] = p\sigma_c^2\,, \tag{50}$$
$$E[p_{k,j}a_{k,j}p_{k,j}c_{k,j}] = pE[a_{k,j}c_{k,j}] = p\sigma_{ca}^2\,. \tag{51}$$

The proof is ended by including these new expectations in Propositions 9 and 10.

References

[1] Y. Sit, C. Sturm, L.Reichardt, T. Zwick, and W. Wiesbeck, "The OFDM joint radar-communication system: An overview," in *International Conference on Advances in Satellite and Space Communications*. Budapest, Hungary: IARIA, Apr. 2011, pp. 69–74.

[2] L. Zheng, M. Lops, Y. Eldar, and X. Wang, "Radar and communication coexistence: An overview," *IEEE Signal Processing Magazine*, vol. 36, no. 5, pp. 85–99, Sep. 2019.

[3] F. Liu, C. Masouros, A. Petropulu, H. Griffiths, and L. Hanzo, "Joint radar and communication design: Applications, state-of-the-art, and the road ahead," *IEEE Transactions on Communications*, vol. 68, no. 6, pp. 3834–3862, Jun. 2020.

[4] Z. Feng, Z. Fang, Z. Wei, X. Chen, Z. Quan, and D. Ji, "Joint radar and communication: A survey," *China Communications*, vol. 17, no. 1, pp. 1–27, Jan. 2020.

[5] D. Ma, N. Shlezinger, T. Huang, Y. Liu, and Y. Eldar, "Joint radar-communications strategies for autonomous vehicles," *IEEE Signal Processing Magazine*, pp. 85–97, Jul. 2020.

[6] K. Fazel and S. Kaiser, *Multi-carrier and spread spectrum techniques (From OFDM and MC-CDMA to LTE and WiMAX)*, 2nd ed. England: John Wiley & Sons Ltd, 2008.

[7] B. Nuss, J. Mayer, and T. Zwick, "Limitations of MIMO and multi-user access for OFDM radar in automotive applications," in *MTT-S International Conference on Microwaves for Intelligent Mobility*, Apr. 2018, pp. 1–4.

[8] J. Wang, B. Zhang, and P. Lei, "Ambiguity function analysis for OFDM radar signals," in *International Conference on Radar*, Oct. 2016, pp. 1–5.

[9] M. Richards, *Fundamentals of Radar Signal Processing*, 2nd ed. McGraw-Hill, 2014.

[10] G. Lellouch, A. Mishra, and M. Inggs, "Impact of the Doppler modulation on the range and Doppler processing in OFDM radar," in *Radar Conference*, Cincinnati, OH, USA, May 2014, pp. 0803–0808.

[11] S. Hanbali, "A review of radar signals in terms of Doppler tolerance, time-sidelobe level, and immunity against jamming," *International Journal of Microwave and Wireless Technologies*, vol. 10, no. 10, pp. 1134–1142, 2018.

[12] Z. He, Y. Yang, W. Chen, and D. Weng, "Range resolution improvement of GNSS-based passive radar via incremental Wiener filter," *IEEE Geoscience and Remote Sensing Letters*, vol. early access, pp. 1–5, Nov. 2021.

[13] D. Weissman, B. Jersak, and L. Staton, "Reduction of interfering signals in swept-frequency radar measurements using complex Wiener filtering," in *Internatioanl Geoscience and Remote Sensing Symposium*, vol. 1, Vancouver, Canada, Jul. 1989, pp. 170–170.

[14] N. Luong, X. Lu, D. Hoang, D. Niyato, and D. Kim, "Radio resource management in joint radar and communication: A comprehensive survey," *IEEE Communications Surveys and Tutorials*, vol. 23, no. 2, pp. 780–814, 2021.

[15] J. Zhang, M. Rahman, K. Wu, X. Huang, Y. Guo, S. Chen, and J. Yuan, "Enabling joint communication and radar sensing in mobile networks. a survey," *IEEE Communications Surveys and Tutorials*, vol. 24, no. 1, pp. 306–345, Firstquarter 2022.

[16] T. Pollet, P. Spruyt, and M. Moeneclaey, "The BER performance of OFDM systems using non-synchronized sampling," in *IEEE Global Communications Conference*, vol. 1, San Francisco, CA, USA, Dec. 1994, pp. 253–257.

[17] T. Pollet, M. Bladel, and M. Moeneclaey, "BER sensitivity of OFDM systems to carrier frequency offset and Wiener phase noise," *IEEE Transactions on Communications*, vol. 43, no. 2–4, pp. 191–193, 1995.

[18] IEEE Std 802.11, *Wireless LAN Medium Access Control (MAC) and Physical Layer (PHY) Specifications*, IEEE Standard Association, New York, NY, USA, Dec. 2016.

[19] G. Franken, H. Nikookar, and P. van Genderen, "Doppler tolerance of ofdm-coded radar signals," in *European Radar Conference*, Manchester, UK, Sep. 2006, pp. 108–111.

[20] J. Navarro-Ortiz, P. Romero-Diaz, S. Sendra, P. Ameigeiras, J. Ramos-Munoz, and J. Lopez-Soler, "A survey on 5G usage scenarios and traffic models," *IEEE Communications Surveys and Tutorials*, vol. 22, no. 2, pp. 905–929, Feb. 2020.

[21] N. Levanon, "Multifrequency complementary phase-coded radar signal," *IEE Proceeding of Radar, Sonar and Navigation*, vol. 147, no. 6, pp. 276–284, Dec. 2000.

[22] V. Riché, S. Méric, J.-Y. Baudais, and E. Pottier, "OFDM signal design for range ambiguity suppression in SAR configuration," in *IEEE International Geoscience and Remote Sensing Symposium*, Munich, Germany, Jul. 2012, pp. 2156–2159.

[23] T. Zhang and X.-G. Xia, "Ofdm synthetic aperture radar imaging with sufficient cyclic prefix," *IEEE Transactions on Geoscience and Remote Sensing*, vol. 53, no. 1, pp. 394–404, 2015.

[24] S. Weinstein, "The history of orthogonal frequency-division multiplexing," *IEEE Communications Magazine*, vol. 47, no. 11, pp. 26–35, Nov. 2009.

[25] F. Harris, "On the use of windows for harmonic analysis with the discrete Fourier transform," *Proceeding of the IEEE*, vol. 66, no. 1, pp. 51–83, Jan. 1978.

[26] S. Kaiser, "On the performance of different detection techniques for OFDM-CDMA in fading channels," in *IEEE Global Communications Conference*, vol. 3, Singapore, Nov. 1995, pp. 2059–2063.

[27] S. Verdú, *Multiuser detection*. New York: Cambridge University Press, 1998.

[28] B. Benmeziane, J.-Y. Baudais, S. Méric, and K. Cinglant, "Comparison of ZF and MF filters through PSLR and ISLR assessment in automotive OFDM radar," in *European radar conference*, Excel, London, UK, Apr. 2022, pp. 1–4.

[29] R. Ash and C. Doléans-Dade, *Probability and Measure Theory*, 2nd ed. Academic Press, 2000.